Optical, structural, and morphological properties of PANI/CdSe(TPs) nanocomposite thin films

Article *in* Journal of Materials Science Materials in Electronics · May 2017

DOI: 10.1007/s10854-017-7079-z

6 authors, including:

Ganesh Bhand
Savitribai Phule Pune University
13 PUBLICATIONS **8** CITATIONS
SEE PROFILE

Ashwini Rohom
Savitribai Phule Pune University
26 PUBLICATIONS **46** CITATIONS
SEE PROFILE

Priyanka Londhe
Savitribai Phule Pune University
27 PUBLICATIONS **62** CITATIONS
SEE PROFILE

Nandu Chaure
Savitribai Phule Pune University
121 PUBLICATIONS **1,256** CITATIONS
SEE PROFILE

J Mater Sci: Mater Electron
DOI 10.1007/s10854-017-7079-z

Optical, structural, and morphological properties of PANI/CdSe(TPs) nanocomposite thin films

Ganesh R. Bhand[1] · Manorama G. Lakhe[1] · Ashwini B. Rohom[1] · Priyanka U. Londhe[1] · Sulabha K. Kulkarni[2] · Nandu B. Chaure[1]

Received: 10 January 2017 / Accepted: 4 May 2017

Abstract Polyaniline (PANI) thin films and cadmium selenide tetrapods (CdSe TPs) have been prepared by low-cost chemical bath deposition and solvothermal route, respectively. Hybrid PANI/CdSe(TPs) nanocomposite layers were obtained by dipping the PANI layers into the solution of CdSe(TPs) for various duration. The optical, structural, morphological and compositional properties of pristine PANI and nanocomposite layers are studied. The dipping time of PANI layer into CdSe(TPs) solution significantly affect onto the above properties. The absorption and PL intensities for PANI/CdSe(TPs) layers in visible to NIR region increases upon increasing the dipping time. CdSe TPs revealed hexagonal crystal structure by X-ray diffraction analysis. The inter-planer distance was measured about 0.352 nm corresponds to (002) plane of hexagonal CdSe with HRTEM. Growth of void free, granular, and densely packed PANI/CdSe(TPs) layers was confirmed from SEM images. Stoichiometric atomic percentage contents of Cd and Se were obtained by EDAX analyses in PANI/CdSe(TPs) thin film. FTIR results indicate the interaction between CdSe and the acid protonated N–H groups of PANI. The LO1 peak of CdSe and increased relative intensity of C–N^+ band of PANI observed in the Raman spectra demonstrates the formation of PANI/CdSe nanocomposites. Thermogravimetric result reveals enhanced thermal stability of PANI/CdSe(TPs) nanocomposite compared to pristine PANI.

✉ Nandu B. Chaure
n.chaure@physics.unipune.ac.in

[1] Department of Physics, Savitribai Phule Pune University (formerly University of Pune), Pune 411007, India

[2] Department of Physics, Indian Institute of Science Education and Research, Dr. Homi Bhaba Road, Pune 411008, India

1 Introduction

The development of inorganic/polymer hybrid nanocomposite have attracted significant attention due to their wide range of potential applications in light emitting diodes [1], super capacitors [2], sensor [3, 4], solar cells [5] and biological studies [6]. The dispersion of nanoparticles in a suitable polymer has emerged as an important area of research because the properties of materials can be tuned to meet the desired applications. The nanocomposite organic semiconductor polymers such as polypyrole, poly(phenylene vinylene) (PPV), polyaniline (PANI) and polythiophenes with various nanoparticles are reported [4–7]. Among these polymers, PANI is widely studied material because of its high electrical conductivity [7, 8], good environmental stability and can be synthesized using economical raw materials [9]. PANI has unique electrical, optical and optoelectronic properties which can be controlled by varying the oxidation state of the main chain and protonation [10]. The formation of PANI films by chemical bath deposition onto glass substrates have been investigated by various groups [11–13]. Several device applications of PANI include anticorrosion coatings [14], electrochromic displays [15], electrodes for light emitting diodes [16], capacitors [17] and photovoltaic devices [18] have been studied. The nanoparticles have a high surface to volume ratio which can modify the optical, electrical and dielectric properties of polymers. Kaner and co-workers [19] synthesized PANI/Au composites and studied the charge transfer effect on the PANI/Au nanoparticles for memory system. The enhanced optical and electrical properties of PANI/CNT/CdS nanocomposites have been studied by Goswami et al. [20]. The inorganic nanostructures synthesized by different methods include colloidal precipitation method [21, 22], solvothermal route [23], sol–gel [24], etc. The

Published online: 13 May 2017

nanostructures of controlled size and shape can be prepared by solvothermal technique [25]. Several reports on the synthesis of composite containing PANI with inorganic nanoparticles such as CdS [26], ZnO [27], CdSe [28], and TiO_2 [29] have been demonstrated. CdSe nanoparticles have received a great deal of attention because of their unique optical and electrical properties [30] suitable for solar cells applications. Recently, Verma et al. [31] studied the electrochemical interaction between CdTe and CdSe nanoparticles with PANI. Xi et al. [32] reported the enhancement in photoluminescence by incorporation of CdS nanowire in PANI matrix. Pandey and coworkers [33, 34] reported the enhanced optical, chemical, and thermogravimetric properties of PANI/CdS composite layers. Landi et al. [35] studied the incorporation of CdSe nanoparticles into poly(3-octylthiophene) conducting polymer, which favors the charge dissociation at the interface. In the dispersion of CdS in PANI matrix, the variation in the interaction by van der Waals interaction or electrostatic interaction has been studied by Sahoo et al. [36]. Therefore, the homogenous dispersion of CdSe into polymer matrix is a critical problem for synthesis of an effective nanocomposite with the enhanced properties.

In the present work, we have reported the synthesis of CdSe tetrapod (TPs), PANI thin films and PANI/CdSe nanocomposite thin films. The optical, structural and morphological properties are studied in detail.

2 Experimental details

2.1 Materials and reagents

Aniline, hydrochloric acid (HCl), ammonium dichromate (ADC), cadmium oxide (CdO) (99.99%), selenium powder (100 mesh, 99.5%), trioctylphopsphine oxide (TOPO), trioctylphosphine (TOP) (technical grade, 95%), chloroform, methanol and oleic acid (OA) were purchased from Sigma-Aldrich. Double distilled water was used as a solvent for preparation of PANI thin films.

2.2 Synthesis of PANI film

A thin layer of PANI has been prepared by the procedure reported by Tokarskya et al. [11] with some modification. Aniline, hydrochloric acid and ammonium dichromate was used to prepare the PANI layers by chemical bath deposition technique. Two solutions were prepared separately, the first one containing aniline and hydrochloric acid dissolved in 80 ml double distilled water (DDW) (served as cationic source) and second one containing ammonium dichromate dissolved in 20 ml DDW at room temperature (act as oxidizing agent). The polymerization of the aniline was started at room temperature by rapidly mixing the solution of ammonium dichromate in aniline precursor. The mixture was stirred continuously at ~150 rpm. After 30 min, a layer was deposited on glass substrate which was rinsed with DDW and subsequently blows with Ar. The obtained films were annealed at 100 °C for 1 h in argon atmosphere to remove the water.

2.3 Synthesis of CdSe NCs

Cadmium selenide (CdSe) nanocrystals have been prepared using solvothermal route. The solutions of selenium (Se) and cadmium (Cd) precursors were prepared separately with two different processes. Firstly, the Se precursor was prepared with 0.6 mM of Se powder and trioctylphosphine (TOP). The mixture was sonica ted at room temperature for few minutes to get the clear transparent solution. Secondly, the matrix consisting 0.3 mM CdO, 0.3 mM TOPO and oleic acid was prepared ~250 °C under nitrogen ambient to produce clear cadmium oleate precursor solution. The solution was allowed to cool to room temperature and the freshly prepared TOP–Se solution was injected into the cadmium oleate solution. The mixture of above solution was transferred in Teflon beaker and sealed in a stainless steel autoclave at 150 °C for 5 h. The autoclave was allowed to naturally cool to room temperature. The final product was centrifuged several times with methanol and chloroform to remove the byproducts and impurities of CdSe solution. Finally, the precipitate was dispersed in chloroform solvent.

2.4 PANI/CdSe nanocomposite layers

Initially, an equivalent amount of CdSe (20 mg in 5 ml chloroform) solution was taken in six beakers. The composite films were prepared by dipping the PANI film in CdSe solution with different duration 15, 30, 60, 120, 300 and 600 s. The films were slowly pulled out from the solution and rinsed with methanol to remove the powdery part. Subsequently these nanocomposite films were annealed at 100 °C in argon ambient for 30 min.

2.5 Characterization techniques

The XRD pattern of CdSe, polyaniline and its composite was recorded with X-ray diffractometer (model D8 ADVANCED Burker, Germany) with CuKα radiation of wavelength $\lambda = 0.154$ nm. Absorption studies were performed by using UV–Vis spectrophotometer (model JASCO V-670). Room temperature Photoluminescence (PL) spectra of the sample were recorded by a spectrophotometer (model Perkin Elmer LS-55, UK). Surface morphology and elemental composition of nanocomposite

films were studied by using a field emission scanning electron microscopy (FESEM) model HITACHI-S4800. The structure of CdSe tetrapods ware studied by using a transmission electron microscopy (TEM) model TECNAI G^2 with an accelerating voltage 200 kV. Fourier transform infrared (FTIR) spectra were recorded on JASCO FT/IR-6100 spectrometer. Raman spectra were recorded by Raman spectrometer (model Renishaw Invia, Raman microscope) at room temperature, fitted with the Argon ion laser of excitation wavelength 785 nm. TGA measurement of pristine PANI and PANI/CdSe(TPs) nanocomposite samples was performed on a Metter Toledo TGA/DSC system from 20 to 750 °C at a heating rate 20 °C/min under nitrogen atmosphere.

3 Results and discussion

3.1 Characterizations of CdSe TPs

The optical absorption and PL spectra of CdSe TPs is shown in Fig. 1. The sharp optical absorption peak of CdSe TPs is exhibited at 540 nm, which is blue shifted to the reported absorption of bulk CdSe (~710 nm). This blue shift is due to the quantum confinement effect of CdSe quantum dots (QDs) [30]. The PL spectra shows a strong band-edge emission peak attributed at 558 nm, which is reasonably narrow and no deep trap emission band in the red spectral region. The calculated full width half-maximum (FWHM) was 34 nm. The narrow FWHM supports good size distribution or mono-dispersity achieved in the nanocrystals.

Figure 2 shows the TEM image of CdSe tetrapods (TPs) prepared by solvothermal technique. Uniform size tetrapods

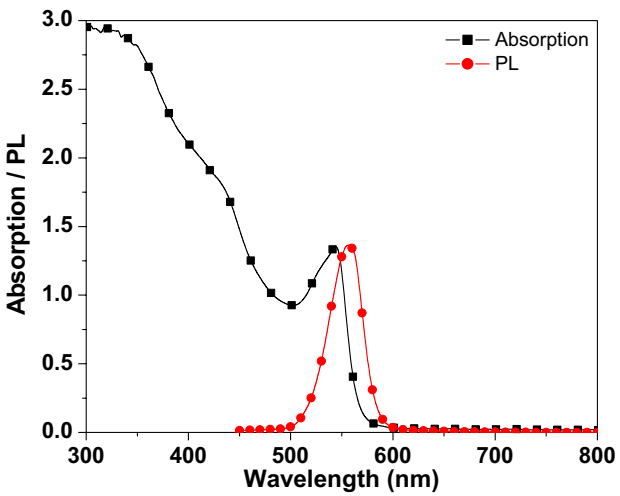

Fig. 1 Absorption and PL spectra of CdSe TPs. (Color figure online)

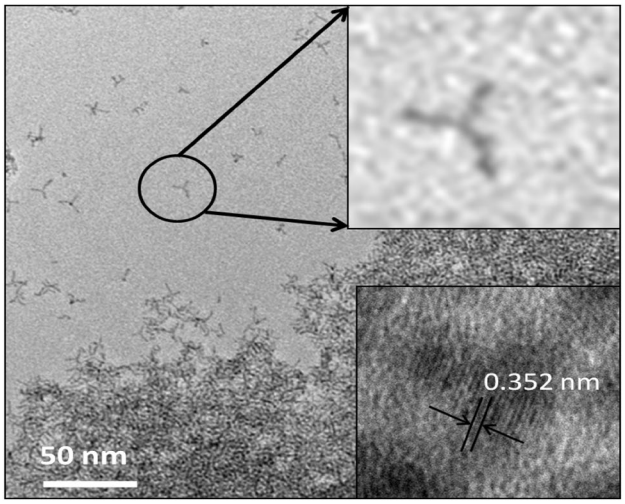

Fig. 2 TEM image of CdSe TPs. *Inset* show the HRTEM image of tetrapod-shaped CdSe

are prepared. The TPs selectivity was up to 90% for statistical number of 100. The main average arm length and width were ~7–8 nm and ~2 nm, respectively. The HRTEM image of CdSe TPs is shown in inset in Fig. 2 exhibits clear lattice fringes separated by 0.352 nm, corresponding to (002) plane of hexagonal wurtzite structure of CdSe. The elemental concentration of CdSe TPs was determined using EDAX technique. Highly stoichiometric CdSe TPs were prepared with atomic percentage concentrations of each element close to 50%.

3.2 Characterizations of PANI/CdSe nanocomposite thin films

3.2.1 Reaction mechanism

Emeraldine salt (dark green) polyaniline thin films formed by chemical polymerization method. Polyaniline/CdSe nanocomposite layers are formed by dipping PANI films in CdSe solution for different duration. The possible reaction mechanism for formation of PANI and PANI/CdSe nanocomposite is given as follows Scheme 1.

3.2.2 X-ray diffraction (XRD) analysis

Figure 3 shows the XRD spectrum of the pristine PANI, CdSe and PANI/CdSe nanocomposite thin films. The peak positions of all samples were determined by fitting these bands to Gaussion curve. Pristine PANI (Fig. 3a) reveals a broad peak at $2\theta \sim 24.6°$ corresponds to (200) plane of PANI and broadening of this peak indicates an amorphous nature of polymer [5]. The XRD spectrum of CdSe TPs (Fig. 3b) exhibited peaks at $2\theta = 23.9°$, 25.4°, 27.1°,

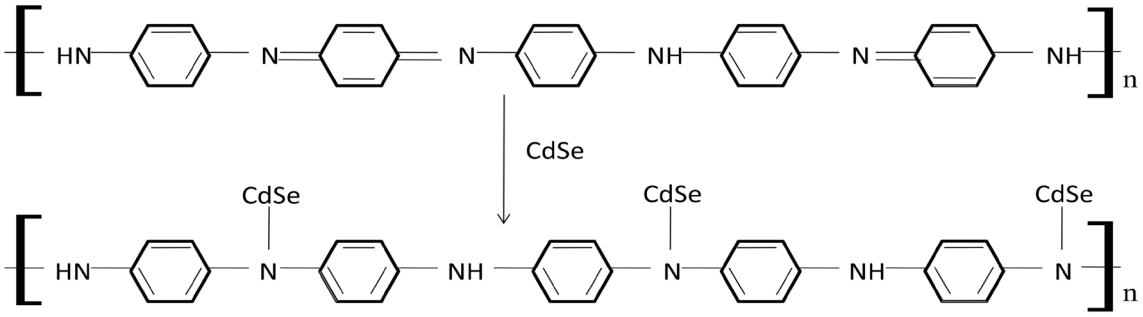

Scheme 1 Proposed mechanism of linking of CdSe TPs with PANI

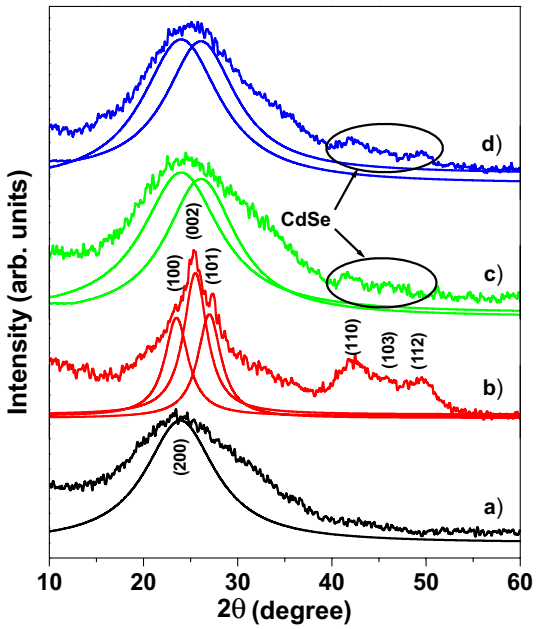

Fig. 3 XRD pattern of PANI (*a*), CdSe TPs (*b*), PANI/CdSe composite 120 s (*c*) and PANI/CdSe composite 600 s (*d*). (Color figure online)

42.2°, 45.6° and 49.6° correspond to (100), (002), (101), (110), (103) and (112) reflection of the hexagonal structure [JCPDS file No. 08-0459]. The broad diffraction peaks of the CdSe are observed due to small size of TPs. CdSe sample was found to be preferentially oriented along (002) plane. Scherrer analysis of CdSe sample estimates the average crystallite size ~6 nm. The XRD pattern of PANI/CdSe nanocomposite the peaks are found to be shifted towards higher 2θ as compared to pristine PANI film (Fig. 3c, d). Furthermore, the intensity of the peak is increased probably due to the interaction between the CdSe and PANI and/or homogeneous distribution of CdSe TPs in the polymer matrix. A similar shift is reported by Pandey and coworkers [33] for PANI/CdS composites. The diffraction pattern in nanocomposite thin films also showed two additional peaks at 2θ ~ 42° and 48°, corresponds to (110) and (112) assigned to the phase of CdSe. This peak supports the formation of PANI/CdSe nanocomposite thin films.

3.2.3 Field Emission Scanning Electron Microscopy (FESEM)

The surface morphology of PANI and PANI/CdSe composite thin film was analyzed using FESEM. Fig. 4a) of pristine PANI film shows compact morphology of grain size ~ 300 to 500 nm with small voids between the grains. Figure 4b, c shows FESEM images of PANI/CdSe nanocomposite layers obtained for 120 and 600 s. In composite, the shape of PANI particle has changed to uniform spherical grain without agglomeration, compact, densely packed films were observed. The change in particles could be associated to the etching of surface of PANI layer in CdSe solution. The enhancement in the compactness of the layer could be due to the incorporation of CdSe TPs to the grain boundaries as the CdSe TPs has high surface energy. The elemental composition of the composite layer was obtained by EDAX analysis. In PANI/CdSe nanocomposite thin films, the presence of Cd and Se was confirmed along with the systematic increases in the contents of Cd and Se with increasing the dipping time. The elemental composition in atomic percentage obtained is represented in Fig. 4d.

3.2.4 Fourier transforms infrared (FTIR) spectra

Figure 5 shows the FTIR spectra of pristine PANI, CdSe and PANI/CdSe nanocomposite thin films. According to the figure PANI spectrum the characteristic absorption bands at 1490 and 1575 cm^{-1} are attributed which corresponds to C=C stretching mode of vibration for the benzenoid and quinoid rings, respectively. The peaks at 1297 and 1240 cm^{-1} are assigned to C–N and C=N stretching vibration of amine [26]. The peak attributed in the range from 1238 to 1245 cm^{-1} is the characteristic of the conducting protonated form of polyaniline. The peak exhibited at 826 cm^{-1} is associated to the out of plane hydrogen deformation of aromatic rings in PANI unit sequences. The

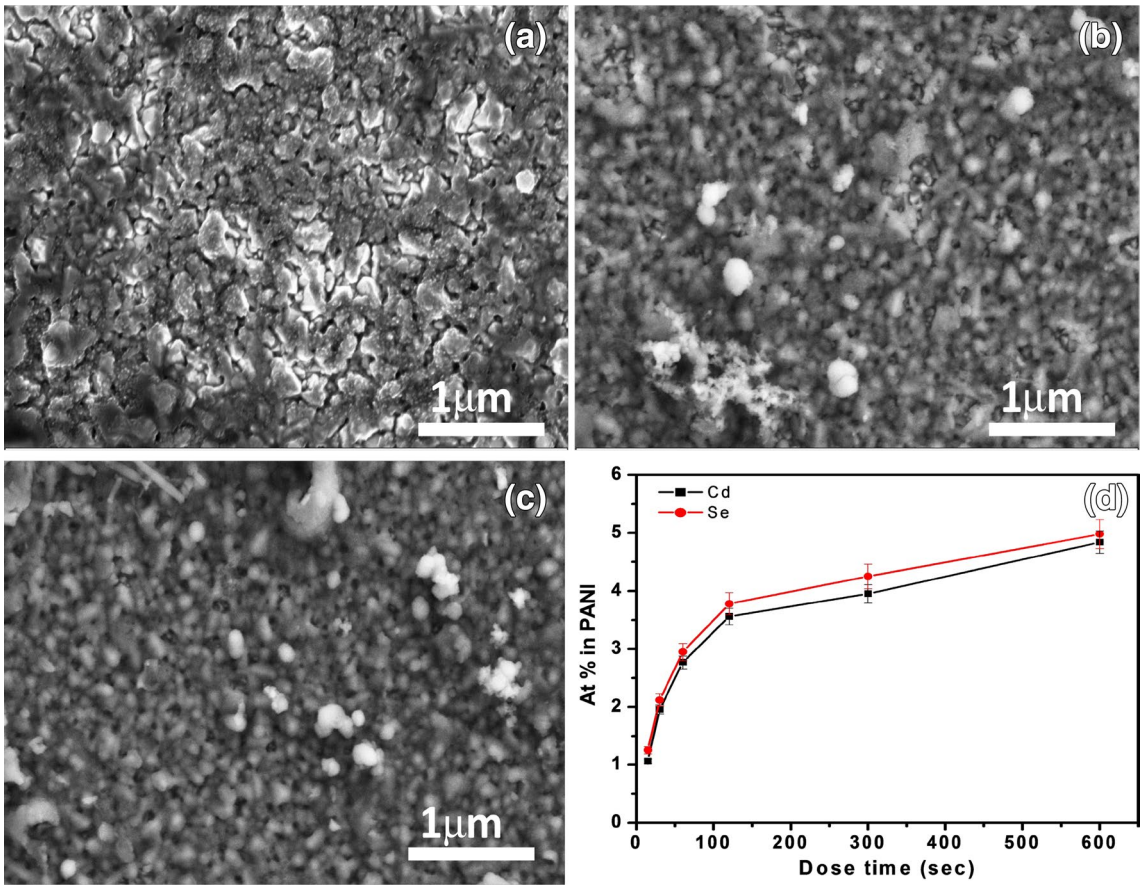

Fig. 4 FESEM image of PANI (**a**), PANI/CdSe 120 s (**b**) and 600 s (**c**) composite thin films. **d** The atomic percentage concentration obtained for PANI/CdSe nanocomposite thin films. (Color figure online)

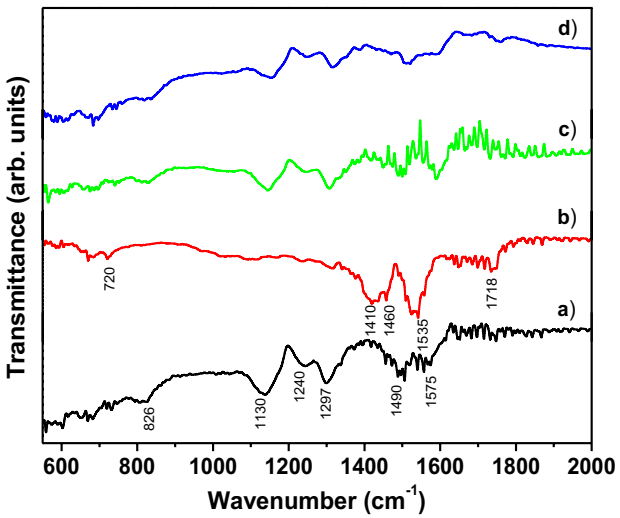

Fig. 5 FTIR spectra of PANI (*a*), CdSe (*b*), PANI/CdSe 120 (*c*) and 600 s (*d*) composite thin films. (Color figure online)

absorption band at 1130 cm^{-1} has been originating from plane bending vibration of C–H.

CdSe spectrum shows the strong signal for the C–H stretching and deformation modes at 1460 and 720 cm^{-1} revealed the presence of alkyl chains. The C=O stretch observed in IR spectrum at 1718 cm^{-1} are due to the oleic acid is present in the CdSe tetrapods. The bands attributed at 1460, 1410 and 1535 cm^{-1} are associated to the characteristic of symmetric and asymmetric stretch, respectively [37]. This result shows that the oleic acid is chemisorbed as a carboxylate onto the CdSe TPs.

However, FTIR spectrum of PANI/CdSe nanocomposite showed broadening of peaks along with shift of some bands to slightly higher or lower values in their positions as compared to pristine PANI. The presence of characteristic IR absorption due to quinoid and benzenoid rings red shift is observed from 1490 and 1575 to 1502 and 1601 cm^{-1}. The peak observed at 1240 cm^{-1} in all PANI/CdSe nanocomposites is related to the C–N stretching mode. The blue shift of CdSe stretching is observed from 720 to 698 cm^{-1} in nanocomposite films can be due to the interaction of CdSe TPs with PANI [5, 38].

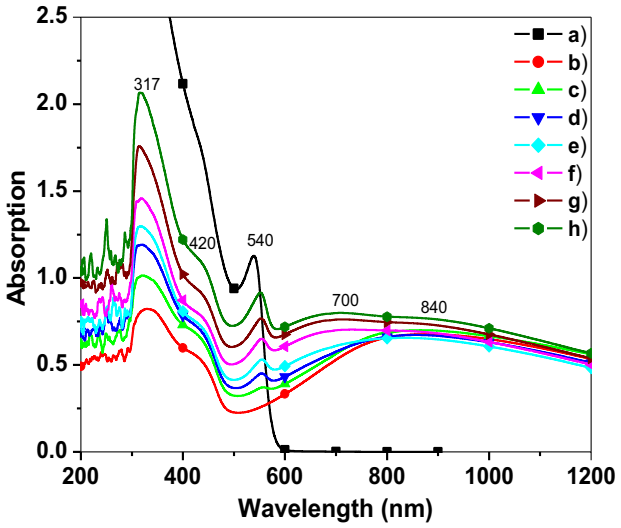

Fig. 6 UV–Vis absorbance spectra of CdSe (*a*), PANI (*b*), PANI/CdSe 15 (*c*), 30 (*d*), 60 (*e*), 120 (*f*), 300 (*g*) and 600 s (*h*) composite thin films. (Color figure online)

3.2.5 Absorption Spectra

UV–Vis absorption spectra of PANI and PANI/CdSe nanocomposite thin films are shown in Fig. 6. PANI films exhibited three distinct absorption bands around 317, 420 and 840 nm, which are associated to π–π* transition of benzonid ring, polaron–π* transition, and π–polaron transition, respectively [8, 39]. The broad band in the near IR region is due to the free charge carriers, characteristic of high electrical conductivity. The UV–Vis spectrum of PANI/CdSe nanocomposite films changes as compared to pristine PANI. The systematic enhancement of absorption from UV–Vis to NIR region after increasing CdSe dose (duration) from 15 to 600 s on PANI films. The relative intensity of first absorption peak attributed at 317 nm of PANI film increases with increasing the dipping time. The corresponding polaron band become flat up to the range from 700 to 840 nm as compared to broad band 840 nm of pristine PANI. This increasing intensity of first absorption peak and flat polaron band in nanocomposite films could be related to the chemical interaction between N–H groups of the PANI chain and CdSe TPs. In nanocomposite layer the CdSe peak is slightly red shifted to 544 nm to 600 s dose. The absorption increases in PANI/CdSe composite from visible region to NIR region with increasing the dipping time of PANI films in CdSe solution. The recorded absorption spectra are broad because of the several transitions in polaron energy band. The results suggest that there is increased interaction between CdSe and PANI films, facilitating faster charge transfer between polymer chain and CdSe.

3.2.6 Photoluminescence (PL) spectra

The PL spectra's of PANI and PANI/CdSe nanocomposite layers excited with wavelength 260 nm are shown in Fig. 7. The observed luminescence peaks are designated as S1, S2, S3, S4, S5, S6 and S7. The S2 emission band, at 384 nm, originates from the π–π* transition of benzenoid units of PANI films [34]. The S1 and S5 emission band at 340 and 472 nm has been attributed to the excitonic and de-excitonic poaron band in all samples. Two small humps S3 and S4 were attributed at 410 and 435 nm could be due to the presence of lighter dopant ions of Cl^- [40]. The PL intensities of nanocomposite film increase with increasing dipping time of PANI films in CdSe solution suggesting that the charge transfer between the electronic levels of PANI and CdSe increases due to the strong interaction between the polymer matrix and the nanoparticles. The S6 emission band observed at 556 nm originated from the CdSe TPs and finally the S7 band observed at 562 nm has been attributed to the PANI/CdSe nanocomposite. The emission peaks of nanocomposite are slightly red shifted compared to corresponding CdSe TPs and small decrease in emission intensity. This observed result can be attributed to the electron transfer from excited CdSe TPs to PANI. The red shift peak in nanocomposite film suggests that light emission feature of CdSe TPs depositing on the surface of PANI [28]. The obtained PL spectrum reveals the formation of PANI/CdSe nanocomposite.

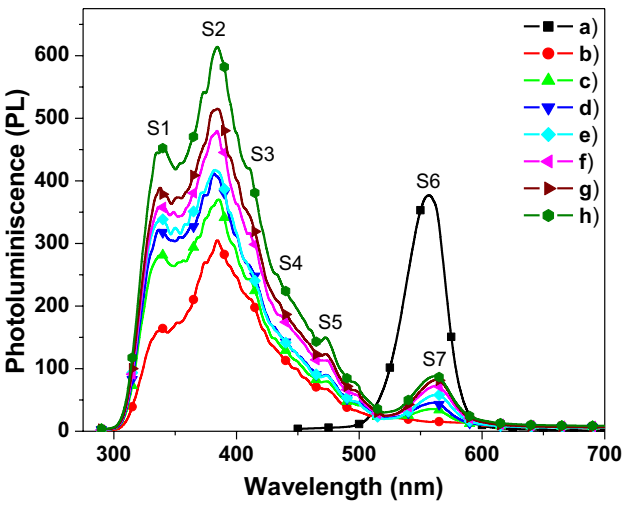

Fig. 7 Photoluminescence spectra of CdSe (*a*), PANI (*b*), PANI/CdSe 15 (*c*), 30 (*d*), 60 (*e*), 120 (*f*), 300 (*g*) and 600 s (*h*) composite thin films. (Color figure online)

3.2.7 Raman spectroscopy

Figure 8 shows the Raman spectra of PANI, CdSe and PANI/CdSe nanocomposite layers. The Raman spectra of PANI layer show a number of peaks whose positions have been marked in the Fig. 8a. According to the spectrum the peaks observed at 1170 and 1227 cm^{-1} can be attributed to C–H bending mode of quinoid and benzenoid rings, respectively [41]. The peak observed at 1343 cm^{-1} has been related to the $C–N^+$ stretching of benzene ring due to the variable protonation and oxidation levels caused by the HCl doping [42]. The peak observed at 1330–1370 and 1500 cm^{-1} corresponds to the C=N stretching and C–H bending of benzene ring. The bands exhibited at 1592 cm^{-1} are associated to the C=C stretching of quinoid and C–C stretching of benzene rings. This stretching vibration mode shows the presence of doped PANI structure [43].

The inset of Fig. 8 shows the Raman spectra of CdSe TPs. The spectra show prominent peaks at ~204 and ~407 cm^{-1} corresponding to the longitudinal optical (LO) phonons modes of 1st order (LO1) and 2nd order (LO2), respectively [44]. The existence of these peaks strongly indicates the high quality of CdSe TPs. The LO1 peak shift toward lower frequency as compared to the bulk CdSe (210 cm^{-1}), these shift is frequently observed for small size NCs due to the effect of spatial confinement of phonons [45]. The low frequency shoulder is observed in LO1 peaks of CdSe sample due to the contribution of the surface optical vibration. These effects are always present in the spectra of small size of the NCs.

The Raman spectra of the PANI/CdSe nanocomposites show similar features as that of PANI with one additional peak at ~204 cm^{-1}, which represents the LO1 peak of CdSe (Fig. 8b–d). Note that the bands at 1170, 1227 and 1592 cm^{-1} are slightly shifted in PANI/CdSe composites. The relative intensity of $C–N^+$ band increased in the PANI/CdSe composites as compared to pure PANI. The increased intensity of 1343 cm^{-1} band indicates the interaction of CdSe TPs with the PANI, which promote the charge transfer properties [19]. The effect in the Raman spectra of composite samples gives a confirm evidence of homogenous dispersion of CdSe in the host polymer matrix and their strong interaction between them. These results are therefore is in good agreement with the absorption spectra discussed earlier (Fig. 6).

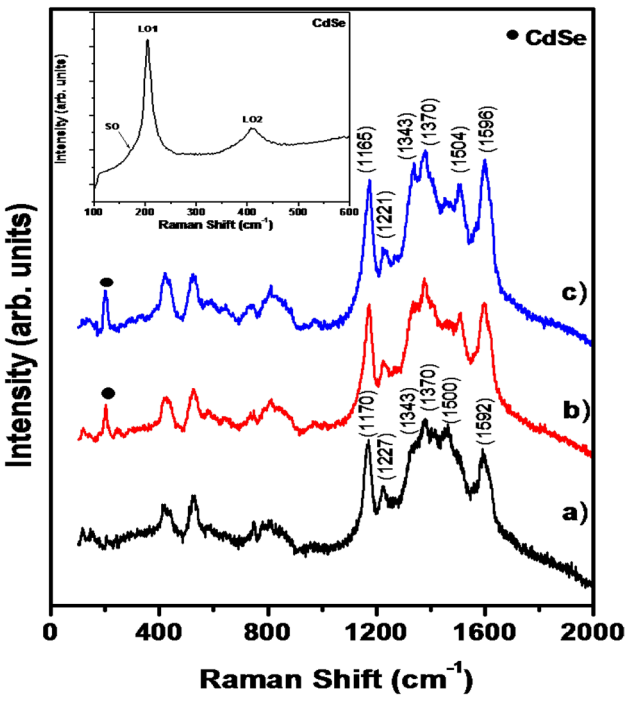

Fig. 8 Raman spectra of pure PANI (*a*), PANI/CdSe 120 (*b*) and 600 s (*c*). *Inset* image shows the Raman spectra of pure CdSe TPs. (Color figure online)

The thermal stability of pristine PANI and PANI/CdSe(TPs) nanocomosite layers was studied by TGA in nitrogen ambient is shown in Fig. 9. A similar decomposition trend with gradual weight loss in both the samples has been observed. Three weight loss steps are exhibits in both the samples. The weight loss observed from room temperature (40) to 125 °C is proposed due to the evaporation of moisture/adsorbed water molecules from the polymer matrix [46]. The second weight loss observed between approximately 140 and 300 °C corresponds to the removal of HCl dopant and un-reacted monomer [47]. The third major weight loss exhibited after 380 °C indicates

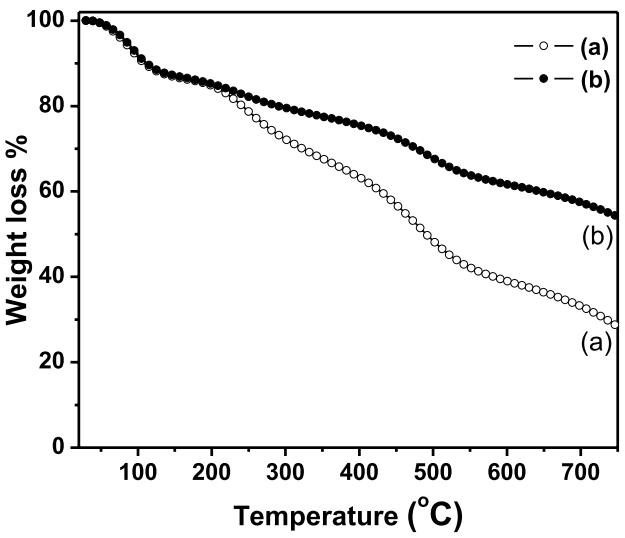

Fig. 9 Thermogravimetric analysis of pristine PANI (*a*) and PANI/CdSe(TPs) nanocomposite (*b*) samples

the structural decomposition of the polymer [48]. The left over residual masses at 750 °C for pristine PANI and PANI/CdSe(TPs) nanocomposite were measured 30 and 56%, respectively. The improved thermal stability in nanocomposite is proposed to be associated to the interaction between PANI and Q-CdSe.

4 Conclusions

In summary, we have reported the synthesis and thorough characterizations of PANI, CdSe(TPs) and hybrid PANI/CdSe(TPs) nanocomposite layer. Uniform, monodispersed CdSe TPs are synthesized by low-cost solvothermal method. A dip coating technique was found to be suitable to prepare uniform PANI/CdSe(TPs) nanocomposite layers. XRD analyses revealed hexagonal structure of CdSe TPs. HRTEM measures the inter-planer distance about 0.352 nm corresponds to (002) plane of hexagonal wurtzite structure of CdSe. The formation of PANI/CdSe nanocomposite thin layers was also confirmed from XRD results. PANI/CdSe(TPs) layers were void free, granular, compact, and densely packed. The elemental composition obtained by EDAX confirms the stoichiometric presence of Cd and Se. Furthermore, the contents of Cd and Se were found to be increased systematically with increasing the dipping time. FTIR results indicate the interaction between CdSe and the acid protonated N–H groups of PANI. The absorption of PANI/CdSe composite layer was found to be increased in visible to NIR region with increasing the dipping time. Furthermore the broad nature of absorption spectra in nanocomposite layer is proposed due to the several transitions in polaron energy bands. The increased PL intensity of nanocomposite layers upon increasing the dipping time reveals the increase of charge transfer between the electronic levels of PANI and CdSe. The LO1 peak of CdSe and increased relative intensity of $C–N^+$ band of PANI observed in the Raman spectra indicates the formation of PANI/CdSe composites. The enhanced thermal stability revealed for PANI/CdSe(TPs) nanocomposite is proposed due to the interaction between PANI and CDSe TPs.

Acknowledgements The financial support received from DST (SERI), Grant No. DST/TM/SERI/FR/124(G) is gratefully acknowledged. GRB is thankful to University Grant Commotions (UGC) for BSR fellowship.

References

1. T. Pandiyarajan, R.V. Mangalaraja, B. Karthikeyan, Spectrochim. Acta A **147**, 280–285 (2015)
2. L. Ma, L. Su, J. Zhang, D. Zhao, C. Qin, Z. Jin, K. Zhao, J. Electroanalytical Chem. **777**, 75–84 (2016)
3. V. Kumar, V. Patil, A. Apte, N. Harale, P. Patil, S. Kulkarni, Langmuir **31**, 13247–13256 (2015)
4. Z. Pang, Z. Yang, Y. Chen, J. Zhang, Q. Wang, F. Huang, Q. Wei, Colloids Surf. A **494**, 248–255 (2016)
5. S. Singh, R.S. Deol, M.L. Singla, D.V.S. Jain, Sol. Energy Mater. Sol. Cells **128**, 231–239 (2014)
6. M.A.M. Youssef, S.A. Mohamed, M.S. Abdel-Aziz, M.E. Abdel-Aziz, G. Turky, S. Kame, Carbohydr. Polym. **147**, 333–343 (2016)
7. M.A. Drury, S. Chaure, M. Kroll, V. Nicolosi, N. Chaure, W.J. Blau, Chem. Mater. **19**, 4252–4258 (2007)
8. B.T. Raut, P.R. Godse, S.G. Pawar, M.A. Chougule, V.B. Patil, J. Phys. Chem. Solids **74**, 236–244 (2013)
9. C.D. Batich, H.A. Laitinen, H.C. Zhou, J. Electrochem. Soc. **137**, 883–885 (1990)
10. D. Verma, V. Dutta, J. Phys. Condens. Matter **19**, 186212–186217 (2007)
11. J. Tokarskya, L. Kulhankovaa, K.M. Kutlakovaa, P. Peikertovaa, J. Svatuškab, V. Styskalab, V. Matejkaa, V. Vasinekb, P. Capkova, Thin Solid Films **537**, 58–64 (2013)
12. J. Stejskal, I. Sapurina, Pure Appl. Chem. **77**, 815–826 (2005)
13. R.M. Rajapakse, A.D. Chandani, L.P. Lankeshwara, N.L. Kumarasiri, Synth. Met. **83**, 73–76 (1996)
14. G.S. Goncalves, A.F. Baldissera, L.F. Rodrigues, E.M.A. Martini, C.A. Ferreira, Synth. Met. **161**, 313–323 (2011)
15. M.A.C. Nwanya, C.J. Jafta, P.M. Ejikeme, P.E. Ugwuoke, M.V. Reddy, R.U. Osuji, K.I. Ozoemena, F.I. Ezema, Electrochim. Acta **128**, 218–225 (2014)
16. H. Wang, J. Lin, Z.X. Shen, J. Sci. 1, 225–255 (2016)
17. N. Chen, Y. Ren, P. Kong, L. Tan, H. Feng, Y. Luo, Appl. Surf. Sci. **392**, 71–79 (2017)
18. D. Geethalakshmi, N. Muthukumarasamy, R. Balasundaraprabhu, Measurement **92**, 446–452 (2016)
19. R.J. Tseng, C.O. Baker, B. Shedd, J. Huang, R.B. Kaner, J. Ouyang, Y. Yang, Appl. Phys. Lett. **90**, 053101–053104 (2007)
20. M. Goswami, R. Ghoshb, T. Maruyamac, A. Meikapa, Appl. Surf. Sci. **364**, 176–180 (2016)
21. D.W. Ayele, W. Su, H. Chou, C. Pan, B. Hwang, Appl. Surf. Sci. **322**, 177–184 (2014)
22. G.R. Bhand, P.U. Londhe, A.B. Rohom, N.B. Chaure, Adv. Sci. Lett. **20**, 1112–1115 (2014)
23. Y. Leng, W. Wang, L. Zhang, F. Zabihi, Y. Zhao, J. Supercritical Fluids **91**, 61–67 (2014)
24. L. Goncalves, F. Kanodarwala, J.A. Stride, C.J. Silva, M.R. Pereira, M. Gomes, J. Photochem. Photobiol. A **285**, 21–29 (2014)
25. Q. Wang, D. Pan, S. Jiang, X. Ji, L. An, B. Jiang, J. Cryst. Growth **286**, 83–90 (2006)
26. B.T. Raut, M.A. Chougule, A.A. Ghanwat, R.C. Pawar, C.S. Lee, V.B. Patil, J. Mater. Sci. **23**, 2104–2109 (2012)
27. R. Saravanan, E. Sacari, F. Gracia, M.M. Khan, E. Mosquera, V. Gupta, J. Mol. Liq. **221**, 1029–1033 (2016)
28. X. Hu, C. Mao, J. Song, H. Niu, S. Zhang, H. Huang, Biosens. Bioelectron. **41**, 372–378 (2013)
29. P. Ranka, V. Sethi, A. Contractor, Thin Solid Films **615**, 44–55 (2016)
30. L.L. Han, D.H. Qin, X. Jiang, Y.S. Liu, L. Wang, J.W. Chen, Y. Cao, Nanotechnology **17**, 4736–4742 (2006)
31. D. Verma, V. Dutta, J. App. Phys. **105**, 034904–034910 (2009)
32. Y. Xi, J. Zhou, H. Guo, C. Cai, Z. Lin, Chem. Phys. Lett. **412**, 60–64 (2005)
33. V.R. Mehto, D. Rathore, R.K. Pandey, Polym. Compos. **35**, 1864–1874 (2014)
34. B.T. Raut, P.R. Godse, S.G. Pawar, M.A. Chougule, D.K. Bandgar, V.B. Patil, Measurement **45**, 94–100 (2012)

35. B.J. Landi, C.S. Castro, H.J. Ruf, C.M. Evans, S.G. Bailey, R.P. Raffaelle, Sol. Energy Mater. Sol. Cells **87**, 733–746 (2005)
36. N.G. Sahoo, S. Rana, J.W. Cho, L. Li, S.H. Chan, Progr. Polym. Sci. **35**, 837–867 (2010)
37. R.K. Beri, P.K. Khanna, CrystEngComm. **12**, 2762–3768 (2010)
38. G.K. Paul, A. Bhaumik, A.S. Patra, S.K. Bera, Mater. Chem. Phys. **106**, 360–363 (2007)
39. C.W. Lee, Y.H. Seo, S.H. Lee, Macromolecules **37**, 4070–4074 (2004)
40. V.J. Babu, S. Vempati, S. Ramakrishna, Mater. Sci. Appl. **4**, 1–10 (2013)
41. M. Baibarac, M. Cochet, M. Lapkowski, L. Mihut, S. Lefrant, I. Baltog, Synth. Met. 96, 63–70 (1998)
42. M.A.G. MacDiarmid, W. Zheng, MRS Bull. **22**, 24–31 (1997)
43. M. Baibarac, I. Baltog, S. Lefrant, J. Solid State Chem. **182**, 827–835 (2009)
44. N. Tschirner, H. Lange, A. Schliwa, A. Biermann, C. Thomsen, K. Lambert, R. Gomes, Z. Hens, Chem. Mater. **24**, 311–318 (2012)
45. L. Lu, X. Xu, W. Liang, H. Lu, J. Phys. **19**, 406221–406231 (2007)
46. M.M. Nobrega, V.L. Martins, R.M. Torresi, M.L.A. Temperini, J. Phys. Chem. C **118**, 4267–4274 (2014)
47. Y. Haldorai, V.H. Nguyen, J. Shim, Colloid Polym. Sci. **289**, 849–854 (2011)
48. M.A.B. Afzal, M.J. Akhtar, M. Nadeem, M.M. Hassan, J. Phys. Chem. C **113**, 17560–17565 (2009)